SOLUTIONS FOR TRIANGULARLY DISTRIBUTED HARMONIC LOADINGS ON AXIALLY SYMMETRIC AREA IN LAYERED HALF-SPACE

G.-S. Liou*

Department of Civil Engineering
National Chiao-Tung University
Hsinchu, Taiwan

ABSTRACT

The paper is to solve the problem of the response of stratified half-space subjected to triangularly distributed time-harmonic loadings on an axial symmetric area in the stratified half-space. Since the distributed area can be very small, the solution can be employed to deal with the problems of elastodynamics using the fundamental solution method. The advantage of the presented solution over Green function is that no singularity will occur in the presented solution. Some numerical results are given and some conclusions have been made. The presented solution is very efficient in computation.

Keywords: Wave propagation, Fundamental solution, Green function.

1. INTRODUCTION

Ground vibration due to near-by sources has been paid attention to over past several decades. Especially for the sensitive facility and high-tech production equipment, this vibration should be mitigated. Therefore, how to predict the vibration becomes an important subject. Woods and Jedele [1] have collected some observed data and deduced them into a simple formula expressing attenuation phenomenon of ground vibration in term of soil damping and distance between source and observation locations. From more theoretical aspects, Sheng *et al*. [2] and Krylov [3] have employed Euler beam theory to model whole track including sleepers and ballast and then to solve the problem of moving train. Kaynia *et al*. [4] have proposed a more sophisticated analysis model, which takes dynamic interaction into account, to evaluate ground vibration induced by passing trains. Moreover, Karlstrom [5] has employed a refined semi-analytic model to investigate the effect on ground vibration due to accelerating train.

Most of the above analysis model, finite element or boundary element methods are employed to model half-space medium or layered half-space medium. Regarding the analytical approach to evaluate ground vibration due to a specific source, Apsel and Luco [6] have calculated the vibrations at the locations on half-space medium due to a point source (Green Function). Vostroukhov *et al*. [7] have employed integral transform method to obtain ground vibration in layered half-space due to a buried uniform load on a circular area.

Also, Kausel and Peek [8] have employed layer elements to obtain Green function for layered medium. Green function has been the fundamental solution for the boundary element method. However, the singularity situation occurs at the location of source point. Some task of boundary element method is to deal with the singularity problem. The paper is going to obtain the solution for the case of distributing the point (concentrated) load over a small area. Therefore, the singularity problem will disappear.

In the solution process, the distributed loading on an axial symmetric area can be decomposed into an infinite series of Fourier components with respect to azimuth. For each Fourier component, triangular distribution in r-direction is assumed.

To solve the problem mathematically, the whole layered half-space medium is divided into two domains (upper and lower domains), the upper domain is the domain above the level where the external loading is applied, and the other is the lower domains which is below the level. For each domain, the technique of decomposing the loading, which was developed by Liou [9], is employed. The decomposed loading will automatically match the forms of boundary values of general solutions of three dimensional wave equations in cylindrical coordinates for layered stratum. Then, the boundary condition of free surface, attenuation condition, and the continuity conditions of displacement and stress components at the interface of the two domains are imposed to obtain the solution.

The analytical expression for the vibration at a specific location in layered medium will be a form of semi-infinite intergration with respect to wave number k.

And Rayleigh singular pole is in the integration path,

* Corresponding author (gsliou@mail.nctu.edu.tw)

DOI : 10.1017/jmech.2015.38
Copyright © 2015 The Society of Theoretical and Applied Mechanics, R.O.C.
https://doi.org/10.1017/jmech.2015.38 Published online by Cambridge University Press

if no material damping is assumed in the medium. However, if material damping is always assigned in the medium, the singular pole will move away from integration path. From the decaying nature of the integrand with respect to wave number k as proven in Liou's work [10], the vibration can be calculated by integrating only up to a certain upper limit k_u without losing accuracy.

The numerical results for the cases of equal total loading with different distribution areas will be compared each other. This will show the phenomenon of variations of displacement and stress components around the different distribution areas of the total loading. According to the numerical investigation, one can deduce that the solution should be closer to Green function solution as the distribution area is getting smaller. However, no singularity situation will occur in the presented solution.

2. SOLUTIONS FOR DYNAMIC LOADINGS IN LAYERED MEDIUM

The general solution of the differential equations for wave propagation in cylindrical coordinates is independently found for individual layer in layered medium. The displacement and stress continuity conditions at the horizontal interfaces in layered system are then imposed for further expressing the displacement and stress fields in terms of the prescribed dynamic loadings [11]. The prescribed dynamic loadings in layered half-space is shown in Fig. 1. In Fig. 1(a), the shaded area is the region where dynamic loadings are applied. Figure 1(b) shows the distribution pattern in r-direction for each Fourier component.

Arbitrarily prescribed loadings on an axially symmetric area can be expressed in cylindrical coordinates in terms of Fourier components with respect to azimuth as follows:

$$\begin{bmatrix} \bar{\tau}_{rz}(r,\theta) \\ \bar{\sigma}_{zz}(r,\theta) \\ \bar{\tau}_{\theta z}(r,\theta) \end{bmatrix} e^{i\omega t} = \sum_{n=0}^{\infty} \begin{bmatrix} \bar{\tau}_{rz}^{n}(r) \begin{Bmatrix} \cos(n\theta) \\ \sin(n\theta) \end{Bmatrix} \\ \bar{\sigma}_{zz}^{n}(r) \begin{Bmatrix} \cos(n\theta) \\ \sin(n\theta) \end{Bmatrix} \\ \bar{\tau}_{\theta z}^{n}(r) \begin{Bmatrix} -\sin(n\theta) \\ \cos(n\theta) \end{Bmatrix} \end{bmatrix} e^{i\omega t}$$
$$r_1 \le r \le r_2\,,\ z = h_i \tag{1}$$

where superscript n denotes n^{th} Fourier component in the series; ω is frequency. Also, one can define $r_2 - r_1 = 2\varepsilon$ as shown Fig. 1(b). Since the time variation $e^{i\omega t}$ appears on both sides of the equation, it will be omitted hereinafter.

As shown in Fig. 1(b), the external loads are assumed to be triangularly distributed for each Fourier component. Thus, the loading distribution in r-direction can be expressed as follows:

$$\bar{\tau}_{rz}^{n} = h(r)\,p\,,\quad \bar{\sigma}_{zz}^{n} = h(r)\,q\,,\ \text{and}\ \ \bar{\tau}_{\theta z}^{n} = h(r)\,s \tag{2}$$

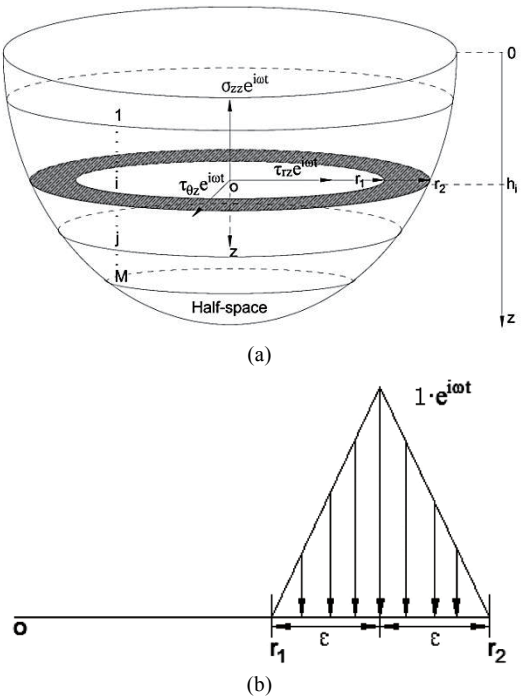


Fig. 1 Total system of layered half-space and triangular load distribution at depth h_i.

where

$$h(r) = \begin{cases} 1 + \dfrac{r - r_0}{\varepsilon} & \text{if } \ r_0 - \varepsilon \le r \le r_0 \\ 1 - \dfrac{r - r_0}{\varepsilon} & \text{if } \ r_0 \le r \le r_0 + \varepsilon \\ 0 & \text{otherwise} \end{cases} \tag{2a}$$

$r_0 = (r_1 + r_2)/2$, p is intensity of distributed load in r-direction, q is intensity in z-direction and s is intensity in θ-direction. The technique developed by Liou [9] is employed to decompose the loadings in Eq. (2). After some mathematical manipulations of solving eigenvalues of Bessel matrix $\boldsymbol{J}$ in Eq. (3b) and Hankel Transform as shown in Liou's work [11], one can obtain the following equations.

$$\boldsymbol{t_n} = \begin{bmatrix} \bar{\tau}_{rz}^{n} \\ \bar{\sigma}_{zz}^{n} \\ \bar{\tau}_{\theta z}^{n} \end{bmatrix} = \int_0^{\infty} \boldsymbol{J} \begin{bmatrix} -D_{n+1} + D_{n-1} & 0 & D_{n+1} + D_{n-1} \\ 0 & D_n & 0 \\ D_{n+1} + D_{n-1} & 0 & -D_{n+1} + D_{n-1} \end{bmatrix} \begin{bmatrix} p \\ q \\ s \end{bmatrix} dk$$
$$= \int_0^{\infty} \boldsymbol{JDP}\, dk \tag{3}$$

where

$$D_{n+1} = \int_{r1}^{r2} \frac{r}{2} J_{n+1}(kr)\, h(r)\, dr$$
$$D_n = \int_{r1}^{r2} r J_n(kr)\, h(r)\, dr \tag{3a}$$
$$D_{n\text{-}1} = \int_{r1}^{r2} \frac{r}{2} J_{n\text{-}1}(kr)\, h(r)\, dr$$

https://doi.org/10.1017/jmech.2015.38 Published online by Cambridge University Press

and

$$\boldsymbol{J}=\begin{bmatrix} J_n'(kr) & 0 & (n/r)\,J_n(kr) \\ 0 & kJ_n(kr) & 0 \\ (n/r)\,J_n(kr) & 0 & J_n'(kr) \end{bmatrix} \tag{3b}$$

where $J_n(kr)$ is first kind of Bessel function of order n, and $J_n'(kr)=[dJ_n(kr)/dr]$.

Since the external loading is applied at level i as shown in Fig. 1(a), the domain is divided into two domains. One is the domain above level i and the other is the domain below level i. Consider the domain below level i in Fig. 1(a) first. As derived in Ref. [11], the displacement and stress components on the upper horizontal surface of a particular layer can be expressed in terms of that on the bottom surface of the layer. Therefore, one can employ the continuity conditions of displacement and stress components from $(i+1)^{th}$ layer down to half-space layer. Then, the displacement and stress components on i^{th} interface (upper surface of $(i+1)^{th}$ layer) can be written as:

$$\boldsymbol{Y}_i=\begin{Bmatrix}\boldsymbol{u}_i\\ \boldsymbol{t}_i\end{Bmatrix}=\begin{bmatrix}\boldsymbol{J} & \boldsymbol{0}\\ \boldsymbol{0} & \boldsymbol{J}\end{bmatrix}\begin{bmatrix}\boldsymbol{T}_{11} & \boldsymbol{T}_{12}\\ \boldsymbol{T}_{21} & \boldsymbol{T}_{22}\end{bmatrix}\begin{bmatrix}\boldsymbol{\kappa}_1'\\ \boldsymbol{\kappa}_2'\end{bmatrix}\boldsymbol{A}' \tag{4}$$

where matrices $\boldsymbol{T}_{11} \sim \boldsymbol{T}_{22}$ are submatrices of transfer matrix $\boldsymbol{T}$, unknown vector $\boldsymbol{A'}=(A,\ B,\ C)^T$ can be determined from the boundary conditions at the surface of half-space, and constitutive matrices $\boldsymbol{\kappa}_1'$ and $\boldsymbol{\kappa}_2'$ are defined in Ref. [11]. After some matrix manipulations of eliminating the unknown vector $\boldsymbol{A'}$, one can obtain the displacement vector $\boldsymbol{u}_i$ in terms of the stress vector $\boldsymbol{t}_i$ as follows:

$$\boldsymbol{u}_i=\boldsymbol{J}(\boldsymbol{T}_{11}\boldsymbol{\kappa}_1'+\boldsymbol{T}_{12}\boldsymbol{\kappa}_2')(\boldsymbol{T}_{21}\boldsymbol{\kappa}_1'+\boldsymbol{T}_{22}\boldsymbol{\kappa}_2')^{-1}\boldsymbol{J}^{-1}\boldsymbol{t}_i=\boldsymbol{JQJ}^{-1}\boldsymbol{t}_i \tag{5}$$

Also, $\boldsymbol{t}_i$ can be expressed in term of $\boldsymbol{u}_i$ as follows:

$$\boldsymbol{t}_i=\boldsymbol{JQ}^{-1}\boldsymbol{J}^{-1}\boldsymbol{u}_i \tag{5a}$$

If the lower domain has a rigid lower boundary, then all the displacement components on lower boundary must be equal to $\boldsymbol{0}$. This leads to $\boldsymbol{Q}=\boldsymbol{T}_{12}\boldsymbol{T}_{22}^{-1}$ for Eqs. (5) and (5a).

Now, consider the upper domain (above level i). The derivation is similar to the derivation (Eqs. (4) ~ (5a)) for lower domain. But the boundary condition is traction free at free surface. Therefore, the displacement-stress vector at free surface can be expressed as

$$\begin{Bmatrix}\boldsymbol{u}_0\\ \boldsymbol{t}_0\end{Bmatrix}=\begin{bmatrix}\boldsymbol{J} & \boldsymbol{0}\\ \boldsymbol{0} & \boldsymbol{J}\end{bmatrix}\begin{bmatrix}\overline{\boldsymbol{T}}_{11} & \overline{\boldsymbol{T}}_{12}\\ \overline{\boldsymbol{T}}_{21} & \overline{\boldsymbol{T}}_{22}\end{bmatrix}\begin{bmatrix}\boldsymbol{J} & \boldsymbol{0}\\ \boldsymbol{0} & \boldsymbol{J}\end{bmatrix}^{-1}\begin{Bmatrix}\boldsymbol{u}_i\\ \overline{\boldsymbol{t}}_i\end{Bmatrix} \tag{6}$$

where $\overline{\boldsymbol{T}}_{11} \sim \overline{\boldsymbol{T}}_{22}$ are submatrices of transfer matrix $\overline{\boldsymbol{T}}$, which can be derived similar to that of $\boldsymbol{T}$ in Eq. (4) [11].

Applying the boundary condition of free surface $\mathbf{t_0}=\boldsymbol{0}$, one can obtain

$$\overline{\boldsymbol{t}}_i=-\boldsymbol{J}\overline{\boldsymbol{T}}_{22}^{-1}\overline{\boldsymbol{T}}_{21}\boldsymbol{J}^{-1}\boldsymbol{u}_i \tag{7}$$

$$\boldsymbol{u}_i=-\boldsymbol{J}\overline{\boldsymbol{T}}_{21}^{-1}\overline{\boldsymbol{T}}_{22}\boldsymbol{J}^{-1}\overline{\boldsymbol{t}}_i \tag{7a}$$

In the derivations (Eqs. (4) ~ (7a)) above, only a specific wave number k has been assumed. For the final solution, all the wave number components have to be summed up together. Therefore, using $\overline{\boldsymbol{t}}_i$ in Eq. (7) and $\boldsymbol{t}_i$ in Eq. (5a), one can conclude that $\boldsymbol{t}_i-\overline{\boldsymbol{t}}_i$ must be equal to the differential of the specific wave number k of n^{th} component of external loading in Eq. (3) due to the stress continuity. This leads to

$$\boldsymbol{t}_i-\overline{\boldsymbol{t}}_i=d\boldsymbol{t}_n \tag{8}$$

where $\boldsymbol{t}_n=\left(\overline{\tau}_{rz}^n(r),\ \overline{\sigma}_{zz}^n(r),\ \overline{\tau}_{\theta z}^n(r)\right)^T$ and $d\boldsymbol{t}_n=\boldsymbol{JDP}dk$ in Eq. (3).

Now, one just substitutes Eqs. (5a), (7) and (3) into Eq. (8) and integrates with respect to k. The following equation is obtained.

$$\boldsymbol{u}_i=\int_0^\infty \boldsymbol{J}\Big[(\boldsymbol{T}_{21}\boldsymbol{\kappa}_1'+\boldsymbol{T}_{22}\boldsymbol{\kappa}_2')(\boldsymbol{T}_{11}\boldsymbol{\kappa}_1'+\boldsymbol{T}_{12}\boldsymbol{\kappa}_2')^{-1}+\overline{\boldsymbol{T}}_{22}^{-1}\overline{\boldsymbol{T}}_{21}\Big]^{-1}\boldsymbol{DP}dk \tag{9}$$

After displacement vector $\boldsymbol{u}_i=(u_r,\ r_z,\ u_\theta)^T$ has been obtained, one can employ Eq. (5a) to calculated the stress vectors $\boldsymbol{t}_i=(\tau_{rz},\ \sigma_{zz},\ \tau_{\theta z})^T$ at level i for lower domain in Fig. 1(a), and Eq.(7) to calculate $\overline{\boldsymbol{t}}_i=(\overline{\tau}_{rz},\ \overline{\sigma}_{zz},\ \overline{\tau}_{\theta z})^T$ at level i for upper domain in Fig. 1(a); *i.e.*

$$\boldsymbol{t}_i=\int_0^\infty \boldsymbol{JQ}^{-1}\Big[(\boldsymbol{T}_{21}\boldsymbol{\kappa}_1'+\boldsymbol{T}_{22}\boldsymbol{\kappa}_2')(\boldsymbol{T}_{11}\boldsymbol{\kappa}_1'+\boldsymbol{T}_{12}\boldsymbol{\kappa}_2')^{-1}+\boldsymbol{T}_{22}^{-1}\boldsymbol{T}_{21}\Big]^{-1}\boldsymbol{DP}dk \tag{10}$$

and

$$\overline{\boldsymbol{t}}_i=\int_0^\infty -\boldsymbol{J}\overline{\boldsymbol{T}}_{22}^{-1}\overline{\boldsymbol{T}}_{21}\Big[(\boldsymbol{T}_{21}\boldsymbol{\kappa}'+\boldsymbol{T}_{22}\boldsymbol{\kappa}_2')(\boldsymbol{T}_{11}\boldsymbol{\kappa}'+\boldsymbol{T}_{12}\boldsymbol{\kappa}_2')^{-1}+\overline{\boldsymbol{T}}_{22}^{-1}\overline{\boldsymbol{T}}_{21}\Big]^{-1}\boldsymbol{DP}dk \tag{10a}$$

In the derivations above, one should note that $\boldsymbol{u}_i$ in Eq. (9) and $\boldsymbol{u}_i$ in Eq. (5) represent the total solution of all wave numbers k and the solution for a specific wave number k, respectively.

Since the displacement vector $\boldsymbol{u}_i$ and the stress vectors $\boldsymbol{t}_i$ and $\overline{\boldsymbol{t}}_i$ have been obtained, the expressions for the displacement components and stress components on all the horizontal planes in both domains can be derived using the formula similar to Eqs. (4), (6), (9), (10) and (10a).

For the stress components on the vertical cylindrical surface, one can employ the equations derived by Liou [9] as follows:

$$\begin{Bmatrix}\sigma_{rr}(r)\\ \tau_{rz}(r)\\ \tau_{r\theta}(r)\end{Bmatrix}=\int_0^\infty\left(\boldsymbol{J}_1\boldsymbol{J}^{-1}\begin{Bmatrix}\tau_{rz}(r,k)\\ \sigma_{zz}(r,k)\\ \tau_{\theta z}(r,k)\end{Bmatrix}+\boldsymbol{J}_2\boldsymbol{J}^{-1}\begin{Bmatrix}u_r(r,k)\\ u_z(r,k)\\ u_\theta(r,k)\end{Bmatrix}\right)dk \tag{11}$$

https://doi.org/10.1017/jmech.2015.38 Published online by Cambridge University Press

where

$$\boldsymbol{J}_1 = \begin{bmatrix} 0 & -kJ_n(kr) & 0 \\ J_n'(kr) & 0 & \dfrac{n}{r}J_n(kr) \\ 0 & 0 & 0 \end{bmatrix}, \tag{11a}$$

$$\boldsymbol{J}_2 = \begin{bmatrix} 2G\left(-\dfrac{J_n'(kr)}{r}+\dfrac{n^2}{r^2}J_n(kr)\right) & 0 & 2G\left(\dfrac{n}{r}J_n'(kr)-\dfrac{n}{r^2}J_n(kr)\right) \\ 0 & 0 & 0 \\ 2G\left(\dfrac{n}{r}J_n'(kr)-\dfrac{n}{r^2}J_n(kr)\right) & 0 & 2G\left(-\dfrac{J_n'(kr)}{r}+\left(\dfrac{n^2}{r^2}-\dfrac{k^2}{2}\right)J_n(kr)\right) \end{bmatrix}, \tag{11b}$$

matrix $\boldsymbol{J}$ is defined in Eq. (3b), G is shear modulus and u_r, u_z, u_θ, τ_{rz}, σ_{zz} and $\tau_{\theta z}$ are the differential displacement and stress components with respect to wave number k on horizontal plane at the same location where σ_{rr}, τ_{rz} and $\tau_{r\theta}$ are being calculated.

In Eq. (11b), one may observe that some elements in matrix $\boldsymbol{J}_2$ is infinite as $r \to 0$ for $n \geq 1$. However, if the Bessel functions in the elements are expressed in terms of polynominal functions, one can conclude that the infinite terms will be cancelled out each other in the elements. This means that there is no infinite element in matrix $\boldsymbol{J}_2$ for $r = 0$.

3. NUMERICAL ANALYSIS

The solutions presented in the paper have been verified with Green function solution [6] for the case of distributed loading applied at free surface. To the cases of distributed loads buried in layered half-space, two types of media have been chosen for numerical analysis. One is a layer over rigid bedrock. The other is half-space. For the medium of one layer over rigid bedrock, the nondimensional layer thickness $\bar{h} = h\,\omega / 2\pi / Re(Cs) = 0.5$, in which C_s is shear wave velocity in the layer, ω is frequency, and h is thickness of the layer. For the two types of media, the distributed loadings are buried at nondimensional depth of $\bar{h}_i = h_i\ \omega / 2\pi / Re(Cs) = 0.15$, Poisson ratio is 0.33, and hysteretic damping ratio is 0.05. In order to investigate the concentration effect of the loadings, three distributed areas are selected. Referring to Fig. 1(b), first case is $\bar{r}_1 = 0.125$ and $\bar{r}_2 = 0.375$ ($\bar{\varepsilon} = 0.125$) in which $\bar{r}_1 = r_1\ \omega / 2\pi / Re(Cs)$ and $\bar{r}_2 = r_2\ \omega / 2\pi / Re(Cs)$; second case is $\bar{r}_1 = 0.2$ and $\bar{r}_2 = 0.3$ ($\bar{\varepsilon} = 0.05$); third case is $\bar{r}_1 = 0.225$, $\bar{r}_2 = 0.275$ ($\bar{\varepsilon} = 0.025$). In order to make the magnitude of total loadings equal among the three cases, the highest intensities are 1.0 for case 1 ($\bar{\varepsilon} = 0.125$), 2.5 for case 2 ($\bar{\varepsilon} = 0.05$) and 5.0 for case 3 ($\bar{\varepsilon} = 0.025$). Figure 2 show the real and imaginary parts of stress component σ_{zz} on the horizontal plane at nondimensional depth $\bar{h}_i = 0.15$ for the case of one layer system and symmetric Fourier component $n = 0$. The external loading for Fig. 2 is applied at $\bar{h}_i = 0.15$ and in z-direction. In the figures, one can observe six curves representing the results at the surfaces of both upper and lower domains for $\bar{\varepsilon} = 0.125$, 0.05 and 0.025 respectively. From Fig. 2(a), one can see that the differences between upper and lower domain surfaces significantly occurs at the locations where external distributed loading is applied, and the differences at $\bar{r} = 0.25$ are 5.0 for $\bar{\varepsilon} = 0.025$, 2.5 for the case of $\bar{\varepsilon} = 0.05$ and 1.0 for $\bar{\varepsilon} = 0.125$. These 5.0, 2.5, and 1.0 are the highest intensities of distributed loadings for the three cases, respectively. Referring to Fig. 2(a), one can observe that stress component in the region, where external load is applied, is smaller for the surface of upper domain. Also, from Figs. 2(a) and 2(b), one can observe the stress continuity at the interface of upper and lower domains. In Fig. 2(b), one can also see that the imaginary part of the stress component is almost the same for $\bar{r} \geq 0.4$. Figure 3 show the stress component τ_{rz} on the horizontal plane at $\bar{h}_i = 0.15$ for the case of half-space and symmetric Fourier component

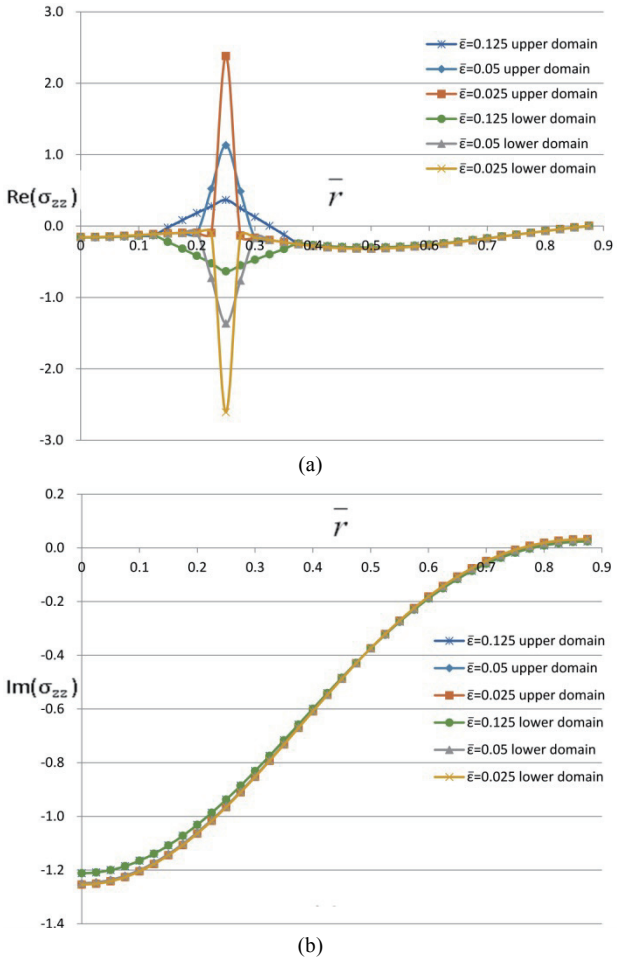


Fig. 2 Stress component σ_{zz} for the case of one layer over rigid bedrock, $\bar{h}_i = 0.15$ and $n = 0$.

https://doi.org/10.1017/jmech.2015.38 Published online by Cambridge University Press

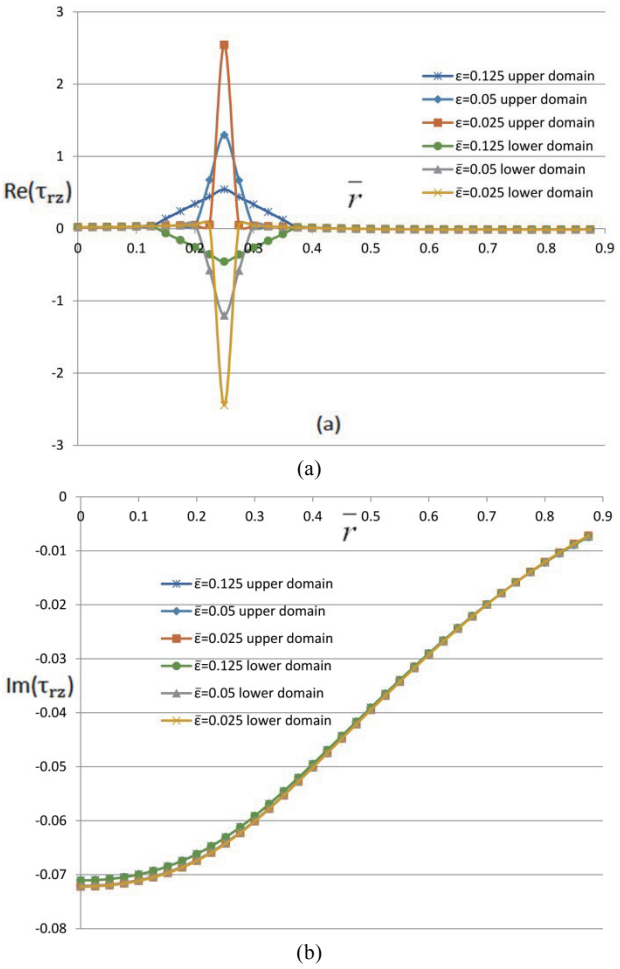


Fig. 3 Stress component τ_{rz} for the case of half-space, $\bar{h}_i = 0.15$ and $n = 1$.

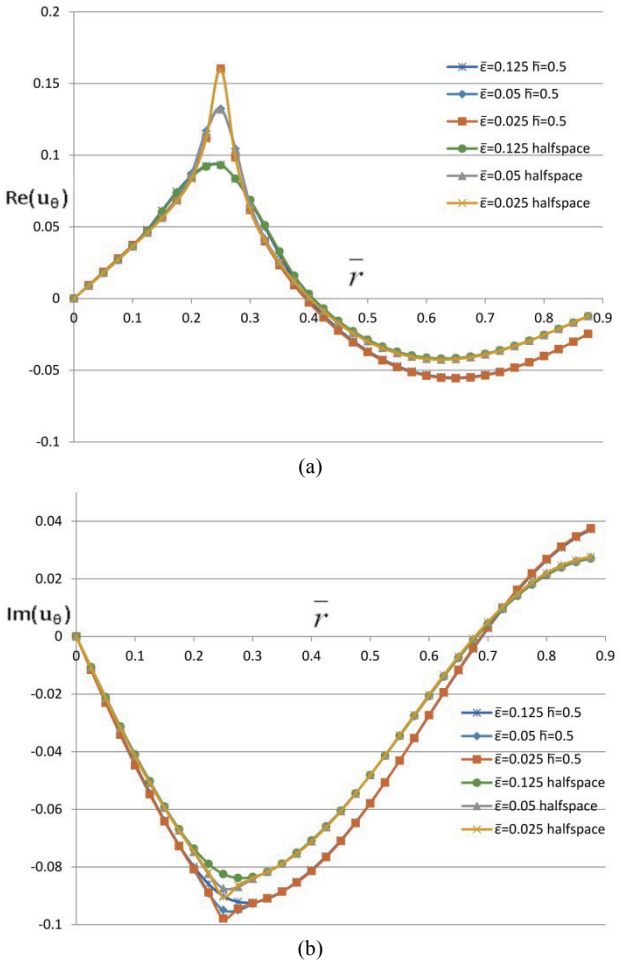


Fig. 4 Displacement component u_θ for the cases of one-layer system and half-space, $\bar{h}_i = 0.15$ and $n = 0$.

$n = 1$. The external loading is applied at $\bar{h}_i = 0.15$ and in r-direction. From the figures, one can observe the similar phenomena to that of Fig. 2. Figure 4 show the displacement u_θ on horizontal plane at $\bar{h}_i = 0.15$ for the cases of both one layer system and half-space, and anti-symmetric Fourier component $n = 0$ is assumed. The external loading is applied at non-dimensional depth $\bar{h}_i = 0.15$ and in θ-direction. From Fig. 4(a), one can see that the maximum displacement occurs at the location of highest intensity of external loading. This phynomenon can also be observed in Figs. 2(a) and 3(a). The displacement values are getting closer to each other as $\bar{r}$ is farther away from the location, where the distributed loading is applied, for the three cases of $\bar{\varepsilon} = 0.125$, 0.05, and 0.025. Also, the difference between the results for the cases of one layer system and half-space is getting apparent as $\bar{r}$ becomes farther. Figure 5 show the displacement component u_z on the horizontal surface at $\bar{h}_i = 0.15$ for the cases of both one-layer system and half-space, and symmetric Fourier component $n = 1$ is assumed. The external loading is applied at nondimensional depth $\bar{h}_i = 0.15$ and in z-direction.

From Fig. 5, one can also see that the displacement is getting closer for the three different cases of $\bar{\varepsilon} = 0.125$, 0.05 and 0.025, if $\bar{r}$ becomes farther. Larger difference observed in Fig. 5(a) among the cases of $\bar{\varepsilon} = 0.125$, 0.05 and 0.125 only occurs at region where external loading is applied. From Figs. 2 ~ 5, one can observe that the peak value is higher as the distributed loading is more concentrated.

In order to know the effect of trunction of integrations in equations like Eq. (9), Table 1 shows the results of τ_{rz} on the horizontal surface at $\bar{h}_i = 0.15$ for the case of one-layer system with $\bar{\varepsilon} = 0.05$. The external loading is applied at $\bar{h}_i = 0.15$ and in r-direction for the table. In the table, nondimensional wave number k_u is employed to replace the infinite integration limit (∞) in equations like Eq. (9). The nondimensional wave number is nondimemsionalized by shear wave velocity and frequency; *i.e.* $k_u = kCs/\omega/2\pi$. Table 1 only shows the results on the surface of lower domain. From the table, one can observe that the results for $k_u = 2000$, 4000 and 6000 are almost the same up to three significant figures. This means that $k_u = 2000$ to replace infinite integration limit is good enough for

https://doi.org/10.1017/jmech.2015.38 Published online by Cambridge University Press

Table 1 Comparisons for different upper limits to replace infinite limit.

$\bar{r}$	Ku = 2,000		Ku = 4,000		Ku = 6,000	
	$\mathrm{Re}(\tau_{rz})$	$\mathrm{Im}(\tau_{rz})$	$\mathrm{Re}(\tau_{rz})$	$\mathrm{Im}(\tau_{rz})$	$\mathrm{Re}(\tau_{rz})$	$\mathrm{Im}(\tau_{rz})$
0	–2.0557E-02	–7.2478E-02	–2.0212E-02	–7.2478E-02	–2.0242E-02	–7.2478E-02
0.05	–1.7410E-02	–7.1925E-02	–1.7439E-02	–7.1925E-02	–1.7441E-02	–7.1925E-02
0.1	–9.4035E-03	–7.0248E-02	–9.4475E-03	–7.0248E-02	–9.4485E-03	–7.0248E-02
0.15	1.8174E-03	–6.7380E-02	1.8087E-03	–6.7380E-02	1.8092E-03	–6.7380E-02
0.2	1.5111E-02	–6.3233E-02	1.3278E-02	–6.3233E-02	1.2659E-02	–6.3233E-02
0.25	1.2559E+00	–5.7773E-02	1.2597E+00	–5.7773E-02	1.2609E+00	–5.7773E-02
0.3	9.6355E-03	–5.1138E-02	7.7783E-03	–5.1138E-02	7.1583E-03	–5.1138E-02
0.35	–6.5068E-03	–4.3658E-02	–6.5238E-03	–4.3658E-02	–6.5243E-03	–4.3658E-02
0.4	–1.7917E-02	–3.5753E-02	–1.7931E-02	–3.5753E-02	–1.7932E-02	–3.5753E-02
0.45	–2.5373E-02	–2.7803E-02	–2.5373E-02	–2.7803E-02	–2.5373E-02	–2.7803E-02
0.5	–2.9013E-02	–2.0098E-02	–2.9005E-02	–2.0098E-02	–2.9008E-02	–2.0098E-02
0.55	–3.0040E-02	–1.2856E-02	–3.0038E-02	–1.2856E-02	–3.0038E-02	–1.2856E-02
0.6	–2.9475E-02	–6.2413E-03	–2.9478E-02	–6.2413E-03	–2.9478E-02	–6.2413E-03
0.65	–2.7913E-02	–3.7733E-04	–2.7915E-02	–3.7733E-04	–2.7915E-02	–3.7733E-04
0.7	–2.5670E-02	4.6508E-03	–2.5668E-02	4.6508E-03	–2.5668E-02	4.6508E-03
0.75	–2.2933E-02	8.7965E-03	–2.2931E-02	8.7965E-03	–2.2931E-02	8.7965E-03
0.8	–1.9866E-02	1.2051E-02	–1.9866E-02	1.2051E-02	–1.9867E-02	1.2051E-02
0.85	–1.6621E-02	1.4440E-02	–1.6622E-02	1.4440E-02	–1.6622E-02	1.4440E-02

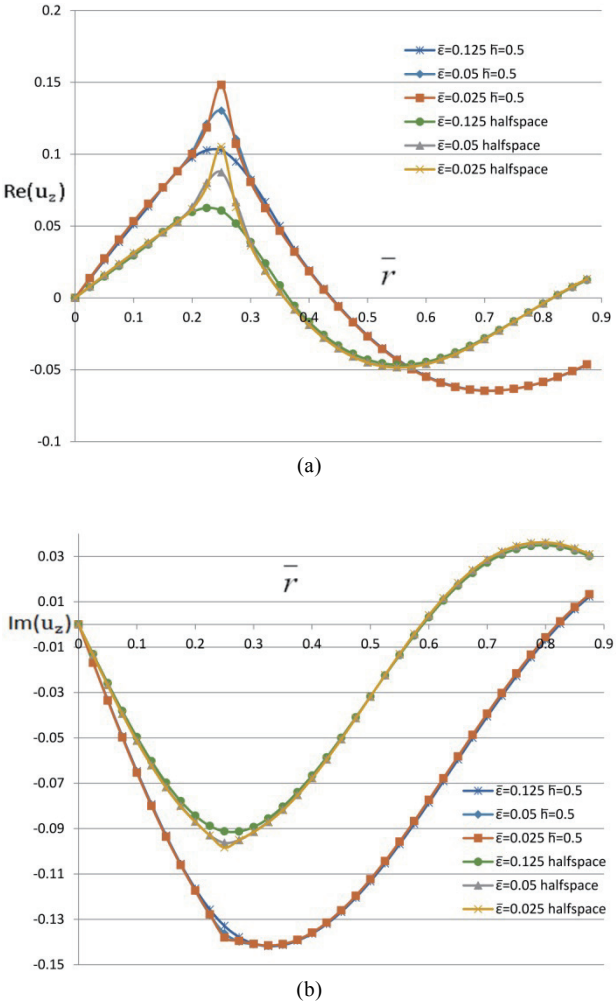


Fig. 5 Displacement component u_z for the cases of one-layer system and half-space, $\bar{h}_i$ = 0.15 and n = 1.

numerical calculations. Although the numerical results for displacement components are not shown, the precision is even much better. For example, in this case, the number of significant figures is five.

Table 2 shows the vertical variation of stress component $\tau_{r\theta}$ at $\bar{r}$ = 0.5 for the case of half-space and anti-symmetric Fourier component n = 0 is assumed. The external loadings are applied in θ-direction and at $\bar{h}_i$ = 0.15 with 0.125 ≤ $\bar{r}$ ≤ 0.375, 0.2 ≤ $\bar{r}$ ≤ 0.3 and 0.225 ≤ $\bar{r}$ ≤ 0.275 respectively. In the table, the depth $\bar{z}$ has been nondimensionalied by shear wave velocity and frequency like $\bar{r}$. From this table, one can observe that the results have no significant difference among the cases of $\bar{\varepsilon}$ = 0.125, 0.05 and 0.025. In the 3 cases of $\bar{\varepsilon}$, one should notice that the magnitude of total loadings of the 3 cases are equal to each other, but the locations, where the equivalent concentrated loads of the 3 cases are applied, are slightly different.

In the discussions above, the distance parameter $\bar{r}$ is kept in 0 ~ 1.0. For $\bar{r}$ greater than 1.0, the numerical results of displacements and stresses will attenuately oscillate down to small values as $\bar{r} \to \infty$. This phenomenon has been observed up to $\bar{r}$ = 10.0 in the investigation.

4. CONCLUSIONS

After thorough numerical investigations, the presented solution is very efficient in computation. From Figs. 2 ~ 5 and Table 2, the numerical results for different loading regions ($\bar{\varepsilon}$ = 0.125, 0.05 and 0.025) with equal total magnitude converge very fast with respect to distance from loading region. The solutions presented in the paper can be easily employed to solve the problem of elastodynamics by fundamental solution method. The advantage of the presented solution is that no singularity situation could occur in the solution process.

https://doi.org/10.1017/jmech.2015.38 Published online by Cambridge University Press

Table 2 Comparisons for different sizes of loading regions.

$\bar{z}$	$\bar{\varepsilon}$ = 0.125		$\bar{\varepsilon}$ = 0.05		$\bar{\varepsilon}$ = 0.025	
	Re($\tau_{r\theta}$)	Im($\tau_{r\theta}$)	Re($\tau_{r\theta}$)	Im($\tau_{r\theta}$)	Re($\tau_{r\theta}$)	Im($\tau_{r\theta}$)
0	–3.2636E-02	1.3228E-01	–3.4687E-02	1.3361E-01	–3.4985E-02	1.3380E-01
0.05	–5.3397E-02	1.4579E-01	–5.5924E-02	1.4740E-01	–5.6285E-02	1.4764E-01
0.1	–8.4324E-02	1.5891E-01	–8.5763E-02	1.6084E-01	–8.5945E-02	1.6112E-01
0.15	–9.6044E-02	1.7142E-01	–9.3033E-02	1.7366E-01	–9.2651E-02	1.7398E-01
0.2	–7.9734E-02	1.6020E-01	–7.7546E-02	1.6241E-01	–7.7254E-02	1.6272E-01
0.25	–5.7685E-02	1.4652E-01	–5.7205E-02	1.4869E-01	–5.7121E-02	1.4900E-01
0.3	–3.4466E-02	1.3100E-01	–3.5298E-02	1.3313E-01	–3.5395E-02	1.3343E-01
0.35	–1.3334E-02	1.1433E-01	–1.4773E-02	1.1638E-01	–1.4964E-02	1.1668E-01
0.4	4.1721E-03	9.7146E-02	2.6270E-03	9.9105E-02	2.4119E-03	9.9389E-02
0.45	1.7594E-02	8.0058E-02	1.6201E-02	8.1907E-02	1.6002E-02	8.2175E-02
0.5	2.7028E-02	6.3594E-02	2.5892E-02	6.5319E-02	2.5727E-02	6.5570E-02

ACKNOWLEDGEMENTS

The financial support of this research is provided by National Science Council of Taiwan through Contract no. NSC-101-2221-E-009-172. The support is appreciated.

NOMENCLATURE

$\boldsymbol{T}$: Transfer matrix for displacement-stress vectors between upper boundary and lower boundary of lower domain [11].

$\boldsymbol{T}_{11} \sim \boldsymbol{T}_{22}$: Submatrices of Transfer matrix $\boldsymbol{T}$.

$\bar{\boldsymbol{T}}$: Transfer matrix for displacement-stress vectors between upper boundary and lower boundary of upper domain [11].

$\bar{\boldsymbol{T}}_{11} \sim \bar{\boldsymbol{T}}_{22}$: Submatrices of Transfer matrix $\bar{\boldsymbol{T}}$.

$\boldsymbol{\kappa}_1'$: Constitutive matrix for displacement vector on top horizontal surface of half-space [11].

$\boldsymbol{\kappa}_2'$: Constitutive matrix for traction vector on top horizontal surface of half-space [11].

r_1 : Inner radius of region of distributed loading (Fig. 1(b))

r_2 : Outer radius of region of distributed loading (Fig. 1(b))

r_0 : $\dfrac{r_1 + r_2}{2}$ (Fig. 1(b))

$\bar{r}_1$: $\dfrac{r_1 \dfrac{\omega}{2\pi}}{Re(Cs)}$

ω : Frequency

Cs : Shear wave velocity

$\bar{r}_2$: $\dfrac{r_2 \dfrac{\omega}{2\pi}}{Re(Cs)}$

ε : $\dfrac{r_2 - r_1}{2}$

$\bar{\varepsilon}$: $\dfrac{\bar{r}_2 - \bar{r}_1}{2}$

$\bar{r}$: $\dfrac{r \dfrac{\omega}{2\pi}}{Re(Cs)}$

h_i : Depth of buried external loading

$\bar{h}_i$: $\dfrac{h_i \dfrac{\omega}{2\pi}}{Re(Cs)}$

REFERENCES

1. Woods, R. D. and Jedele, L. P., "Energy-Attenuation Relationships from Construction Vibrations," *Proceedings of Vibration Problems in Geotechnical Engineering Convention*, Detroit, Michigan, pp. 229–246 (1985).
2. Sheng, X., Jones, C. J. C., and Petyt, M., "Ground Vibration Generated by a Load Moving Along a Railway Track," *Journal of Sound and Vibration*, **228**, pp. 129–156 (1999).
3. Krylov, V. V., "Vibrational Impact of High-Speed Trains. I. Effect of Track Dynamics," *Journal of the Acoustical Society of America*, **100**, pp. 3121–3134 (1996).
4. Kaynia, A. M., Madshus, C. and Zackrisson, P., "Ground Vibration from High-Speed Trains: Prediction and Countermeasure," *Journal of Geotechnical and Geoenvironmental Engineering*, **126**, pp. 0531–0573 (2000).
5. Anders Karlstrom, "An Analytical Model for Ground Vibrations from Accelerating Trains," *Journal of Sound and Vibration*, **293**, pp. 587–598 (2006).
6. Apsel, R. J. and Luco, J. E., "On the Green's Functions for a Layered Half-Space, Part II," *Bulletin of Seismological Society of America*, **73**, pp. 931–951 (1983).
7. Vostroukhov, A. V., Verichev, S. N., Kok, A. W. M., and Esveld, C., "Steady-State Response of a Stratified Half-Space Subjected to a Horizontal Arbitrary Buried Uniform Load Appied at a Circular Area," *Soil Dynamics and Earthquake Engineering*, **24**, pp. 449–459 (2004).

https://doi.org/10.1017/jmech.2015.38 Published online by Cambridge University Press

8. Kausel, E. and Peek, R., "Dynamic Loads in the Interior of a Layered Stratum: An Explicit Solution," *Bulletin of the Seismological Society of America*, **72**, pp. 1459–1481 (1982).
9. Liou, G.-S., "Analytical Solutions for Soil-Structure Interaction in Layered Media," *Journal of Earthquake Engineering and Structural Dynamics*, **18**, pp. 667–686 (1989).
10. Liou, G.-S., "Vibrations Induced by Harmonic Loadings Applied at Circular Rigid Plate on Half-Space Medium," *Journal of Sound and Vibration*, **323**, pp. 257–269 (2009).
11. Liou, G.-S., "Vibrations Induced by Harmonic Loadings Applied at Circular Plate on Layered Medium," *Journal of Mechanics*, **29**, pp. 197–206 (2013).

(Manuscript received August 19, 2014,
accepted for publication January 13, 2015.)

https://doi.org/10.1017/jmech.2015.38 Published online by Cambridge University Press